High-Pressure Phases of Cordierite From Single-Crystal X-Ray Diffraction to 15 GPa

Gregory J. Finkelstein[1*], Przemyslaw K. Dera[2, 3], and Thomas S. Duffy[1]

[1]Department of Geosciences, Princeton University, Princeton, NJ 08544, USA

[2]Hawaii Institute of Geophysics & Planetology, School of Ocean and Earth Science and Technology, University of Hawaii, 1680 East West Road (POST Bldg 819E), Honolulu, Hawaii 96822, USA

[3]GSECARS, University of Chicago, Building 434A, 9700 South Cass Avenue, Argonne, Illinois 60439, USA

*Email Address: gjfinkel@princeton.edu

Key Words: cordierite; phase transition; crystallography; high pressure; single-crystal X-ray diffraction

Revision 1

Abstract

High-pressure single-crystal X-ray diffraction experiments were conducted on natural cordierite crystals with composition $Mg_{1.907(18)}Fe_{0.127(6)}Al_{4.01(2)}Si_{4.96(3)}Na_{0.026(3)}O_{18.12(9)}$ using a synchrotron X-ray source. The samples were compressed at 300 K in a diamond anvil cell to a maximum pressure of 15.22(15) GPa with a neon pressure-transmitting medium and a gold pressure calibrant. We observed a recently described orthorhombic to triclinic transition, as well as a further transition to a second triclinic phase. We solved and refined both new triclinic phases in space group *P*1, and designate them cordierite II and III. The structures of cordierite II and III were refined at 7.52(3) GPa at 15.22(15) GPa, respectively. The lattice parameters at these pressures are a = 15.567(3) Å, b = 9.6235(4) Å, c = 9.0658(6) Å, α = 89.963(5)°, β = 86.252(10)°, and γ = 90.974(8)° for cordierite II, and a = 8.5191(19) Å, b = 8.2448(3) Å, c = 9.1627(4) Å, α = 85.672(4)°, β = 85.986(7)°, and γ = 70.839(10)° for cordierite III. Across the phase transitions there is a significant reduction in the length of the a-axis (~2 Å per phase transition), whereas both the b- and c-axis remain largely unchanged. Cordierite II has four- and five-coordinated Si and Al, while cordierite III has four-, five-, and six-coordinated Si, four- and five-coordinated Al, and five- and six-coordinated Mg. The sequence of high-pressure phases shows increasing polymerization of coordination polyhedra. These results, together with other recent studies, suggest that mixed 4-, 5-, and 6-fold coordination states may occur more commonly in silicate structures compressed at 300 K than previously recognized.

Introduction

Cordierite is an aluminosilicate framework mineral with ideal stoichiometry of

46 $(Mg, Fe)_2Al_4Si_5O_{18} \bullet (nCO_2, mH_2O)$ that crystallizes in the orthorhombic system (space group
47 *Cccm*, Z = 4) at ambient conditions. It is found widely in metamorphic rocks, and plays an
48 important role as a geothermometer, geobarometer, and monitor of fluid or melt volatile content
49 (Currie 1971; Martignole and Sisi 1981; Carrington and Harley 1996). Due to its low thermal
50 expansivity, it also has widespread use in applications that require high thermal-shock resistance,
51 such as automotive parts and cookware (Hochella et al. 1979; Roy et al. 1989).
52 The cordierite structure consists of a network of tetrahedral (Al^{3+}, Si^{4+}) and octahedral
53 (Mg^{2+}, Fe^{2+}) cation-oxygen coordination polyhedra interspersed with channels that can contain
54 larger molecules (e.g. H_2O, CO_2) or additional cations (e.g. Na^{+}). When the structure is viewed
55 in the *ab* plane, two types of layers, M-layers and T-layers, can be recognized (Figures 1 and 2).
56 M-layers consist of Al/Si rhombic disphenoids (tetrahedra in which all faces consist of
57 equivalent scalene triangles such that opposite edges are equal in length) and Mg/Fe octahedra
58 arranged in six-sided edge-sharing rings, forming a layer of interconnected rings. Within each
59 ring, Al or Si disphenoids are edge-connected on either side to a Mg/Fe octahedron. Within a
60 layer, a given octahedron is connected to two Si disphenoids and one Al disphenoid. T-layers
61 consist of 6-membered rings of corner-sharing Al and Si tetrahedra in a 1:2 ratio that are isolated
62 laterally within a layer, but are cross-linked above and below by corner-sharing with the larger
63 rings in the M-layers (Malcherek et al. 2001). The stacking of rings in the M- and T-layers
64 results in large channels running parallel to the *c*-axis of the structure (Figure 1).
65 At temperatures >1450° C, cordierite adopts a high-temperature hexagonal structure that
66 is isotypic with beryl (space group *P6/mcc)* (Schreyer and Schairer 1961; Putnis 1980a). This
67 phase, called indialite, has Al and Si disordered over a single site (designated T_1) in the M-layers
68 in a 2:1 ratio, and Al and Si disordered over a single site (T_2) in the T-layers in a 1:2 ratio

(Meagher and Gibbs 1977). In low-temperature cordierite, the Al and Si order into distinct sites. The transformation between the hexagonal and orthorhombic phases was shown to occur by an intermediate order-modulated phase (Putnis 1980b). In orthorhombic cordierite, the T_1 site splits into two symmetrically distinct sites, the Al-occupied T_11 site and Si-occupied T_16, and the T_2 site splits into three symmetrically distinct sites, the Al-occupied T_26 site and the Si-occupied T_21 and T_23 sites (Meagher and Gibbs 1977). While Mg and Fe predominantly occupy the M site, Mössbauer spectroscopy has shown that up to 11% of Fe^{2+} can substitute into tetrahedral sites (Malcherek et al. 2001). Fe-rich compositions have also been shown to have less pronounced Al/Si ordering in the M-layers than Mg-rich compositions (Malcherek et al. 2001).

Three large sites are located in the channels along the *c*-axis (Figure 1). One of these sites can be occupied by large cations, such as Na^+ or K^+ (Armbruster 1986). Natural cordierite compositions with significant amounts of Na^+ also typically incorporate some Be^{2+} or Li^+ in the place of Al^{3+} or Mg^{2+}/Fe^{2+}, respectively, in order to maintain charge balance (Armbruster 1986; Bertoldi et al. 2004). Water molecules primarily occupy the other two channel sites, and are designated Type I or II depending on the site. Molecules occupying Type II sites interact with the large channel cations, while Type I occupants do not. The Type I site can also be filled with a variety of other small molecules, the most common of which is CO_2 (Goldman et al. 1977; Armbruster and Bloss 1980; Armbruster 1985; Kolesov and Geiger 2000). Since we will be focusing only on ordered cordierite phases at low temperature here, we simplify the terminology in this paper and designate the M, T_11, T_26, T_16, T_21, T_23, and Type I H_2O sites as the Mg1, Al1, Al2, Si1, Si2, Si3, and Ch1 sites, respectively, (Type II H_2O and Na channel sites are not included in our structure refinements).

There have been only a limited number of previous high-pressure studies on cordierite at 300 K. Most of these studies reached maximum pressures of less than 5 GPa. A major focus has been on how various molecules used as pressure-transmitting media may enter cordierite's channels, modifying the structure's compressibility (e.g., water in pressure-induced hydration) (Mirwald 1982; Mirwald et al. 1984; Koepke and Schulz 1986; Likhacheva et al. 2011; Likhacheva et al. 2013). Recently, Miletich et al. (2014a) carried out a high-pressure single-crystal X-ray diffraction study of cordierite in a diamond anvil cell using a 4:1 methanol-ethanol pressure-transmitting medium. They observed elastic softening in the *b*- and *c*-directions, leading to a structural transition to a phase with a primitive triclinic unit cell above ~7.0 GPa (however, the transition pressure may be dependent on channel volatile content (Miletich et al. 2014b; Scheidl et al. 2014)). The structure of the new phase was not reported. In this study, we use synchrotron-based single-crystal X-ray diffraction techniques to investigate the high-pressure behavior of cordierite to a maximum pressure of 15.22(15) GPa in order to identify and characterize its high-pressure structures.

Experimental Methods

A natural, gem-quality cordierite crystal (variety iolite) of unknown origin was used as the starting material. Small fragments (≤10 μm thick) from a larger crystal were extracted for our experiments. The sample composition was determined from an average of six measurements to be $Mg_{1.907(18)}Fe_{0.127(6)}Al_{4.01(2)}Si_{4.96(3)}Na_{0.026(3)}O_{18.12(9)}$ (on the basis of Al + Si + Mg + Fe = 11) using a JEOL 6500f field-emission scanning electron microscope (SEM) with a silicon drift detector (Table 1). Sodium and the excess oxygen (likely as H_2O or CO_2) are expected to occupy cordierite's channel sites. All iron was assigned as Fe^{2+}, as Mössbauer spectroscopy has shown

114 that the Fe^{3+} content in natural Mg-rich cordierites is no more than 0.004 Fe^{3+} per formula unit
115 (Geiger et al. 2000). However, the presence of a trace amount of Fe^{3+} in our purple-colored
116 sample is likely, as this color in iolite has been attributed to Fe^{2+}-Fe^{3+} intervalence charge
117 transfer (Faye et al. 1968; Goldman et al. 1977).
118 Raman spectra were collected on an un-oriented sample using a Horiba LabRAM HR
119 spectrometer and are consistent with previously reported measurements for cordierite. The major
120 peaks can be assigned to stretching, bending, or more complex vibrations (Figure 3) (Geiger et
121 al. 2000; Kaindl et al. 2011; Haefeker et al. 2012). We observe Raman peaks arising from H_2O
122 and CO_2 in Type I sites, indicating the presence of both types of molecules in the channels. The
123 intensity of the Raman peak from the Type II H_2O stretching mode is detectable, but
124 significantly weaker (Figure 3).
125 Ambient-pressure single-crystal X-ray diffraction measurements were performed on a
126 cordierite sample (Table 2, Run #1) at Northwestern University's Integrated Molecular Structure
127 Education and Research Center (IMSERC) using a Bruker diffractometer with Mo Kα sealed-
128 tube X-ray source, Kappa-geometry goniometer, and Apex2 detector. The measured unit cell
129 parameters for this crystal were a = 17.0508(6) Å, b = 9.7129(3) Å, and c = 9.3357(3) Å and are
130 consistent with literature values (Smyth and McCormick 1995; Malcherek et al. 2001).
131 High–pressure single-crystal X-ray diffraction experiments were performed using a
132 synchrotron X-ray source at the 16-ID-B beamline (HPCAT) of the Advanced Photon Source
133 (APS), Argonne National Laboratory. Two separate experiments were carried out (Table 2). Run
134 #2 consisted of three pressure steps at 1.37(7), 8.30(10), and 15.22(15) GPa, while Run #3
135 consisted of a single data collection at 7.52(3) GPa. The samples were compressed using a 4-pin
136 diamond anvil cell with 300-μm culet diamonds. The Boehler-Almax anvil and seat design

137 (Boehler and De Hantsetters 2004) was used to enhance reciprocal space coverage. Sample
138 chambers were formed by drilling a ~170-μm hole through a rhenium gasket that was pre-
139 indented to ~35-μm thickness. A cordierite crystal (~20 μm x 20 μm x 10 μm) was loaded in the
140 sample chamber together with an annealed ruby sphere and a gold foil (~20-μm thick) for
141 pressure calibration. Neon was loaded as a pressure-transmitting medium using a gas-loading
142 system (Rivers et al. 2008).
143 Pressures were determined based on the gold pressure scale of Fei et al. (2007). The unit
144 cell parameter of gold was determined by least squares refinement of five diffraction lines
145 ((111), (200), (220), (311), and (222)) (Table 2). Pressure uncertainties were estimated from the
146 standard deviation of the lattice parameters determined from the individual diffraction lines.
147 Monochromatic diffraction experiments at HPCAT were performed using X-rays with
148 wavelengths of 0.30622 Å (Run #2) and 0.35145 Å (Run #3) and a focused X-ray beam size of
149 ~4 μm x 5 μm. Diffraction patterns were collected with a MarCCD detector that was calibrated
150 using a LaB_6 standard and the program FIT2D (Hammersley et al. 1996). At each pressure, wide
151 and stepped scans about the vertical axis of the diffractometer (ω scan) were collected. The
152 angular coverage of the wide scans was dictated by the geometry of the diamond cell and
153 consisted of either six consecutive 11° rotations (Run #2) or seven consecutive 10° rotations
154 (Run #3) of the cell while the detector was exposed (covering a total angular range of 66° and
155 70°, respectively). These were used to extract *d*-spacings, azimuthal angles around the beam
156 center, and peak intensities. The step size of the wide scan was chosen to be sufficiently small so
157 as to minimize peak overlap, but large enough to mask small timing errors between the rotation
158 and the X-ray shutter. Stepped scans consisted of individual exposures taken at either 1° (Run
159 #2) or 0.5° (Run #3) intervals to constrain the ω angle of maximum intensity for each peak. This

160 provides the third dimension necessary for reconstructing the crystal's reciprocal lattice and
161 indexing the diffraction pattern. Both wide and stepped scans were collected at the central
162 detector position, as well as at positions horizontally shifted ±70 mm in order to maximize the
163 number of peaks measured. For the same reason, wide and stepped scans were also collected at
164 two χ settings that were 90° apart. The data were merged into a single file using the program
165 XPREP for further processing.

166 Peak fitting was performed using the program GSE_ADA (Dera et al. 2013b).
167 Polarization and Lorentz corrections were applied to the fit peaks. The unit cell and orientation
168 matrix were found using the program CELL_NOW (Bruker AXS Inc.). Transformations to
169 conventional unit cells were determined using XPREP (Sheldrick 2008), and lattice parameters
170 were refined using a least-squares fitting procedure in the program RSV (Dera et al. 2013b).

171 Partial crystal structures were solved using the program XT (Sheldrick 2008). SHELX-
172 2013 (Sheldrick 2008) was then used to compute difference Fourier maps between the observed
173 and calculated structure factors, $F_{observed}$-$F_{calculated,}$ that could be used to identify electron density
174 holes and thereby locate atoms missing in the initial model produced by XT. Final refinements of
175 the full structures were carried out in SHELX at selected pressures. X-ray dispersion corrections
176 were implemented for non-standard X-ray wavelengths using the program XDISP (Kissel and
177 Pratt 1990). CrystalMaker (CrystalMaker Software Ltd.) and Endeavor (Putz et al. 1999) were
178 used for visualization. Coordination polyhedra were assigned based on examination of
179 histograms of cation-oxygen distances.

180 The measured composition of our sample,
181 $Mg_{1.907(18)}Fe_{0.127(6)}Al_{4.01(2)}Si_{4.96(3)}Na_{0.026(3)}O_{18.12(9)}$, shows that there is a slight deficit of Si and
182 excess of Mg/Fe compared with ideal stoichiometry $(Mg, Fe)_2Al_4Si_5O_{18} \bullet (nCO_2, mH_2O)$ (Table

183 1). However, our X-ray diffraction measurement could not resolve these small compositional
184 deviations, so site occupancy factors (SOFs) were fixed at a value of one for all anions and
185 cations except for the octahedral Mg/Fe site in the cordierite refinement at ambient conditions. In
186 this case, the Mg/Fe ratio was refined and resulted in a Mg occupancy of 0.959(4) and Fe
187 occupancy of 0.041(4). For the high-pressure structures, the number of refined parameters was
188 minimized by fixing the site occupancy factors for Mg and Fe at the values determined from the
189 refinement at ambient conditions and only refining a single isotropic thermal displacement
190 parameter (U_{iso}) for all sites related to a given site in the initial cordierite structure.
191 Representative structural data are presented in Tables 3-6.
192
193 **Results and Discussion**
194 Three phases were observed upon compression to 15.22(15) GPa (Figure 4, Table 2). At
195 ambient pressure and 1.37(7) GPa, we observe the cordierite phase while the triclinic phase
196 recently reported by Miletich et al. (2014a) was observed at 7.52(3) and 8.30(10) GPa. A second
197 previously unreported high-pressure phase was found at 15.22(15) GPa (Figure 4). We have
198 refined the initial cordierite structure (Tables 3 and 6) and solved and refined the crystal structure
199 of both the high-pressure phases (Tables 4-6).
200 At ambient conditions, our results for the cordierite are consistent with previously
201 reported refinements (Cohen et al. 1977; Meagher and Gibbs 1977; Miletich et al. 2014a), with
202 R1 of 3.30%. The measured *a* lattice parameters for cordierite at ambient pressure and 1.37(7)
203 GPa (Run #2) show anomalously low compressibility in the *a* direction in comparison with
204 previous work (Miletich et al. 2014a). This behavior is likely to be an artifact due to the use of
205 different instruments for these two measurements.

For the ambient-pressure refinement we had 100% completeness of unique diffraction peaks within the resolution limit of the collected diffraction, but this is not achievable when the sample is compressed in a diamond anvil cell. As a result, at ambient pressure we were able to determine that the constituents of the Ch1 channel site were disordered. This is manifested by the large anisotropic displacement parameters (Table 3). It is likely that the large isotropic displacement parameters we observe in the high-pressure cordierite structures also originate from similar disorder within the channels of those structures. We did not include additional channel sites in the refinement because when added they caused the refinement to become unstable. Omitting additional channel sites is consistent with the measured low Na content of the sample, as well as the weak Type II H_2O Raman peak.

At high pressures, we observe two new structures that we designate cordierite II and III. Both have triclinic *P*1 symmetry. We are able to refine the structures in this space group to R1 values of 7.22% and 6.44% at 7.52(3) and 15.22(15) GPa, respectively. The higher R1 values compared with ambient conditions are likely due to a combination of higher background from the diamond anvil cell and limited coverage in reciprocal space (these factors also contribute to larger uncertainties in refined quantities, such as bond lengths). The unit cell shape of cordierite II is metrically similar to cordierite, but in cordierite III the number of formula units per unit cell is halved. Triclinic unit cells are conventionally reported with all acute or all obtuse angles, but for convenience we report here the structure of cordierite II with the unit cell in an orientation corresponding to that of the cordierite structure, resulting in two acute angles and one obtuse angle (this is a different configuration than was reported in Miletich et al. (2014a)). While we use a conventional primitive triclinic unit cell to report the structure of cordierite III (Tables 2, 5, and 6c), we have opted to compare structural features in the text using a non-conventional *C*1

configuration that can be directly compared with cordierite and cordierite II. The transformation matrix used to relate the conventional primitive unit cell and centered cell is:

$$\begin{bmatrix} 1 & 1 & 0 \\ \bar{1} & 1 & 0 \\ 0 & 0 & 1 \end{bmatrix}$$

A comparison of the three different structures is shown in Figure 1. The cordierite, cordierite II, and cordierite III structures are shown for both the *ab* and *ac* planes at 10^{-4}, 7.52(3), and 15.22(15) GPa, respectively. The primary change in the unit cell between the three structures is a significant reduction in the length of the *a*-axis (~2 Å per phase transition), while both the *b*- and *c*-axis remain largely unchanged in length (Table 2). In addition, the structures adopt progressively higher-coordinated cation polyhedra.

To illustrate the specific changes that occur across each phase transition, it is useful to examine individual layers in the *ac* plane. Figure 2 shows the M and T layers separated into four panels. While the M/T 1 and 2 layers are symmetrically equivalent in the cordierite structure, they are distinct in the cordierite II and III structures.

In cordierite, the M-layers contain octahedrally coordinated Mg and tetrahedrally coordinated Si and Al. In cordierite II, all Mg cations remain in octahedral coordination, but half (Mg1A, Mg1B, Mg1G, Mg1H) move along <010> such that two of the Mg-O bonds that had previously formed part of the backbone of the MgO_6 octahedra, are broken. The shifted Mg cations bond with two additional O anions from the T-layers immediately above and below in <001>. These new bonds complete distorted octahedra around the Mg cations (additional geometric details for polyhedra that undergo changes in coordination at high pressure are provided in Figure 5a/Table 7a and Figure 5b/Table 7b for the M1 and T1 layers, respectively). Al1A/Si1A, Al1B/Si1C, Al1G/Si1B, and Al1H/Si1D, which had formed rhombic disphenoids in cordierite, become either more regular tetrahedra (Al1A, Al1H) or distorted 5-coordinated

trigonal bipyramids (Al-1B, Al-1G, Si-1A, Si-1C, Si-1B, Si-1D) in cordierite II (trigonal bipyramids are defined by an axial angle of 180° and radial angles of 120°). Whereas in cordierite these Al and Si polyhedra are not directly connected to one another, in cordierite II each Al is connected to a Si through either one (Al1A/Si1A, Al1H/Si1D) or two (Al1B/Si1C, Al1G/Si1B) bridging O anions that had been previously bonded to Mg.

In cordierite II, the remaining Mg and Al cation polyhedra (Mg1E, Mg1F, Mg1C, Mg1D, Al1E, Al1F, Al1C, Al1D) are slightly more distorted than those in cordierite. However, on transition to cordierite III, these cations adopt similar configurations as previously described for the Mg and Al cations, such that they become symmetrically equivalent to them. Additional changes are that all Al cations become 5-coordinated, and that all Mg cations, except Mg-1E, lose one bond (Figure 5a) to become 5-coordinated. Both the 5-coordinated Mg and Al polyhedra are closer to distorted square pyramids in shape than to trigonal bipyramids, as neither have any bonds with angles near the 180° required for a trigonal bipyramid configuration. Also, since each Si now has two O anions on either side in ~<100> and <$\bar{1}$00> connecting it to an Al cation, the Si cations are now 6-coordinated in a distorted octahedral configuration.

Compared with the coordination polyhedra in the M-layers, those in the T-layers undergo fewer topological changes across the high-pressure polymorphs. However, the 6-membered Al-Si polyhedral rings that make up the layers become significantly distorted. In cordierite II, the rings remain unconnected, but within each layer half the rings elongate in one direction, and the other half in a direction rotated ~45° in the *ab* plane (~<231>/<1$\bar{4}\bar{1}$> for T1 and ~<2$\bar{3}$1>/<29$\bar{2}$> for T2). This elongation is accompanied by out-of-plane rotation of all the Al/Si tetrahedral members of the rings. In cordierite III, the rings become connected between Si-3A/Si-3B in the T1 layer and Si-3C/Si-3D in the T2 layer to form chains of distorted rings running in <1$\bar{1}$0> in

274 the T1 layer and <110> in the T2 layer. The rings themselves are all elongated the same way
275 within a given layer, but in a different direction than the chains themselves (<$1\bar{4}\bar{1}$> for T1 and
276 <$29\bar{2}$> for T2). The polymerization of the rings results in the silicon atoms, Si3A, Si3B, Si3C,
277 and Si3D adopting a 5-coordinated square pyramid configuration.
278 Figure 6 shows the evolution of coordination polyhedra between the three cordierite
279 polymorphs from the perspective of the *ab* and *ac* planes. This illustrates that as pressure is
280 raised, increased polymerization occurs not just between the Al-Si rings, but also between the
281 individual Si polyhedra. In cordierite, Si occurs only as tetrahedral dimers or isolated tetrahedra.
282 In cordierite II, the tetrahedra that were initially isolated are now 5-coordinated and connected to
283 one of the tetrahedral dimers. In cordierite III, the 5-coordinated Si become 6-coordinated and
284 attached to the other dimer. The tetrahedral dimers also become connected, forming additional 5-
285 coordinated Si polyhedra. This results in infinite continuous chains of 4-, 5-, and 6-coordined Si
286 running in <$10\bar{1}$> (101) that are bridged by two-membered chains of Al polyhedra, consisting of
287 one tetrahedron and one square pyramid each.
288 Recent a*b initio* theoretical calculations predicted that the beryl structure, isotypic with
289 cordierite's high-temperature indialite polymorph, undergoes a transition to a slightly modified
290 triclinic $P\bar{1}$ structure at ~14 GPa and 0 K (Prencipe et al. 2011). The cordierite II and III
291 structures identified here are quite different from the predicted beryl polymorph. The proposed
292 $P\bar{1}$ structure is a comparatively minor modification to the initial hexagonal beryl structure that
293 only involves polyhedral tilting. In the high-pressure cordierite structures, there are significant
294 changes in bonding and coordination polyhedra as described above.
295 An unusual feature of the high-pressure structures we observe is their mixture of Al, Si,
296 and Mg coordination. Five-coordinated Mg and Al are known only in a few minerals each (e.g.

297 grandidierite (Stephenson and Moore 1968), yoderite (Fleet and Megaw 1962), andalusite (Ralph
298 et al. 1984)) and as far as we are aware, there are only two previous experimental reports of a
299 silicate structure with a mix of 4-, 5-, and 6-fold Si coordination polyhedra: the triclinic titanite-
300 like $CaSi_2O_5$ structure observed by Angel et al. (1996) and a high-pressure orthorhombic
301 polymorph of (Mg, Fe)SiO_3 orthopyroxene (Finkelstein et al. In Press). While cation
302 coordination polyhedra with five ligands can adopt either a trigonal bipyramid or square pyramid
303 configuration, in both of the high-pressure structures 5-coordinated Si is found in only a square
304 pyramid configuration.
305 In $CaSi_2O_5$, the triclinic structure was found to transform at ~0.2 GPa to a monoclinic
306 structure that contains both 4- and 6-coordinated Si (Angel 1997). The transformation
307 mechanism involves an oxygen atom switching bonds between Ca and Si, thus lowering the
308 coordination number of Ca and increasing the coordination number of Si (Yu et al. 2013). We
309 observe similar bond-switching between Mg and Si in the M-layers on transition to cordierite II
310 and III that results in 5- and then 6-coordinated Si in these layers. The coordination change of
311 other Si cations, as well as Al, from 4- to 5-fold coordination is similar to what we previously
312 observed in the 4- to 5-coordinated Si transition in the high-P orthopyroxene polymorph. In that
313 case, tilting of members of parallel chains of Si tetrahedra resulted in cross-linking between the
314 chains by 5-coordined Si. This is analogous to the tilting and linking of Si and Al polyhedra in
315 both the M- and T-layers of the cordierite high-pressure phases.
316
317 **Implications**
318 Upon compression of cordierite to 15.22(15) GPa, we observe two new structures:
319 cordierite II at 7.52(3) GPa and cordierite III at 15.22(15) GPa. Both structures are triclinic and

exhibit several interesting features, including mixed 4-, 5-, and 6-fold coordination polyhedra of Mg/Fe, Al, and Si, as well as increasing amounts of polymerization of Si across each transition. Questions that require further study include the energetics of the new phases (are they stable or metastable?) and the effects of different pressure media on the transition pressures and structural parameters.

Until recently, few single-crystal structure refinements existed for complex silicate structures at high pressures. With the development of new synchrotron techniques, it is now possible to more routinely carry out compression experiments at 300-K using single-crystal diffraction on low-symmetry silicates (Dera et al. 2013b; Duffy 2014). At these low temperatures, equilibrium reconstructive transitions are kinetically inhibited. While it was once widely thought that silicates undergo pressure-induced amorphization when compressed at room temperature to high pressures (Richet and Gillet 1997), it is now becoming clear that, in some cases, additional, often metastable, polymorphs can be formed (Plonka et al. 2012; Dera et al. 2013a; Zhang et al. 2013; Finkelstein et al. 2014). It is increasingly apparent from these studies that step-wise changes in the coordination number of polyhedra and increased polymerization of polyhedra with compression may be common features of such transitions.

Acknowledgements

We thank Yue Meng, along with the staffs of HPCAT and IMSERC for assistance with diffraction experiments and John Armstrong and Katherine Crispin of the Carnegie Institution for Science for assistance with SEM measurements. This work was supported by the National Science Foundation. Portions of this work were performed at HPCAT (Sector 16) of the Advanced Photon Source, Argonne National Laboratory. HPCAT is supported by the

343 Department of Energy and the National Science Foundation. Use of the gas-loading system was
344 supported by GSECARS and COMPRES.
345

Figure Captions

Figure 1. The *ab* and *ac* planes of the cordierite, cordierite II, and cordierite III structures at 10^{-4}, 7.52(3), and 15.22(15) GPa, respectively. Si polyhedra are blue, Al polyhedra are orange, and Mg polyhedra are gray. Channel sites are represented by red spheres. For cordierite III, the bold axes show the conventional *P*1 unit cell for comparison with the nonconventional *C*1 configuration used here (thin black lines).

Figure 2. The *ab* planes of cordierite (10^{-4} GPa), cordierite II (7.52(3) GPa), and cordierite III (15.22(15) GPa) are shown as four distinct layers: M1/M2 and T1/T2. Si polyhedra are blue, Al polyhedra are orange, and Mg polyhedra are gray. Channel sites are represented by red spheres.

Figure 3. Raman spectrum of un-oriented cordierite sample at ambient conditions. Major peaks are labeled with the letters s, b, r, and/or o, which correspond to stretching, bending, rotational, and other mode assignments (Kaindl et al., 2011), respectively. H_2O and CO_2 stretching modes are labeled.

Figure 4. Left: Example diffraction pattern for cordierite III at 15.22(15) GPa at the center detector position. The black box indicates the magnified region used to illustrate different cordierite phases on the right. Right: a) *Cccm* cordierite at 1.37(7) GPa. The small spots are diffraction peaks from the cordierite crystal. Also visible are diamond peaks (large spots)

and powder rings from Au, Ne, and DAC components. b) *P*1 cordierite II diffraction at 8.30(10) GPa. c) *P*1 cordierite III diffraction at 15.22(15) GPa.

Figure 5. a) Evolution of coordination polyhedra across cordierite phases in the M1 layer for Mg (gray), Si (blue), and Al (orange). Additional Mg-O, Si-O, and Al-O bonds for high-pressure phases are dark gray, dark blue, and green, respectively. Bonds that are broken across phase transitions are indicated by dotted lines. b) Coordination changes in Si polyhedra in the T1 layer.

Figure 6. Selected portions of the *ab* and *ac* planes of cordierite, cordierite II, and cordierite III at 10^{-4}, 7.52(3), and 15.22(15) GPa, respectively. Si polyhedra are blue and Al polyhedra are orange spheres with black frames. Numeric labels indicate Si coordination number.

References

Angel, R.J. (1997) Transformation of fivefold-coordinated silicon to octahedral silicon in calcium silicate, $CaSi_2O_5$. American Mineralogist, 82(7), 836-839.

Angel, R.J., Ross, N.L., Seifert, F., and Fliervoet, T.F. (1996) Structural characterization of pentacoordinate silicon in a calcium silicate. Nature, 384(6608), 441-444.

Armbruster, T. (1985) Ar, N_2, and CO_2 in the structural cavities of cordierite, an optical and X-ray single-crystal study. Physics and Chemistry of Minerals, 12(4), 233-245.

-. (1986) Role of Na in the structure of low-cordierite: A single-crystal X-ray study. American Mineralogist, 71(5-6), 746-757.

Armbruster, T., and Bloss, F.D. (1980) Channel CO_2 in cordierites. Nature, 286(5769), 140-141.

Bertoldi, C., Proyer, A., Garbe-Schönberg, D., Behrens, H., and Dachs, E. (2004) Comprehensive chemical analyses of natural cordierites: Implications for exchange mechanisms. Lithos, 78(4), 389-409.

Boehler, R., and De Hantsetters, K. (2004) New anvil designs in diamond-cells. High Pressure Research, 24(3), 391-396.

Carrington, D.P., and Harley, S.L. (1996) Cordierite as a monitor of fluid and melt H_2O contents in the lower crust: An experimental calibration. Geology, 24(7), 647-650.

Cohen, J.P., Ross, F.K., and Gibbs, G.V. (1977) An X-ray and neutron diffraction study of hydrous low cordierite. American Mineralogist, 62(1-2), 67-78.

Currie, K.L. (1971) The reaction 3 cordierite = 2 garnet + 4 sillimanite + 5 quartz as a geological thermometer in the Opinicon Lake region, Ontario. Contributions to Mineralogy and Petrology, 33(3), 215-226.

Dera, P., Finkelstein, G.J., Duffy, T.S., Downs, R.T., Meng, Y., Prakapenka, V., and Tkachev, S. (2013a) Metastable high-pressure transformations of orthoferrosilite Fs_{82}. Physics of the Earth and Planetary Interiors, 221, 15-21.

Dera, P., Zhuravlev, K., Prakapenka, V., Rivers, M.L., Finkelstein, G.J., Grubor-Urosevic, O., Tschauner, O., Clark, S.M., and Downs, R.T. (2013b) High pressure single-crystal micro X-ray diffraction analysis with GSE_ADA/RSV software. High Pressure Research, 1-19.

Duffy, T. (2014) Earth science: Crystallography's journey to the deep Earth. Nature, 506(7489), 427-429.

Faye, G.H., Manning, P.G., and Nickel, E.H. (1968) Polarized optical absorption spectra of tourmaline, cordierite, chloritoid and vivianite: Ferrous-ferric electronic interaction as a source of pleochroism. American Mineralogist, 53(7-8), 1174-1201.

Fei, Y., Ricolleau, A., Frank, M., Mibe, K., Shen, G., and Prakapenka, V. (2007) Toward an internally consistent pressure scale. Proceedings of the National Academy of Sciences, 104(22), 9182-9186.

Finkelstein, G.J., Dera, P., Jahn, S., Oganov, A.R., Holl, C.M., Meng, Y., and Duffy, T.S. (2014) Phase transitions and equation of state of forsterite to 90 GPa from single-crystal X-ray diffraction and molecular modeling. American Mineralogist, 99(1), 35-43.

Finkelstein, G.J., Dera, P.K., and Duffy, T.S. (In Press) Phase transitions in orthopyroxene (En_{90}) to 49 GPa from single-crystal X-ray diffraction. Physics of the Earth and Planetary Interiors.

Fleet, S.G., and Megaw, H.D. (1962) The crystal structure of yoderite. Acta Crystallographica, 15(7), 721-728.
Geiger, C.A., Rager, H., and Czank, M. (2000) Cordierite III: the site occupation and concentration of Fe3+. Contributions to Mineralogy and Petrology, 140(3), 344-352.
Goldman, D.S., Rossman, G.R., and Dollase, W.A. (1977) Channel constituents in cordierite. American Mineralogist, 62(11-12), 1144-1157.
Haefeker, U., Kaindl, R., and Tropper, P. (2012) Semi-quantitative determination of the Fe/Mg ratio in synthetic cordierite using Raman spectroscopy. American Mineralogist, 97(10), 1662-1669.
Hammersley, A.P., Svensson, S.O., Hanfland, M., Fitch, A.N., and Hausermann, D. (1996) Two-dimensional detector software: From real detector to idealised image or two-theta scan. High Pressure Research, 14(4-6), 235-248.
Hochella, M.F., Brown, G.E., Ross, F.K., and Gibbs, G.V. (1979) High-temperature crystal chemistry of hydrous Mg- and Fe-cordierites. American Mineralogist, 64(3-4), 337-351.
Kaindl, R., Többens, D.M., and Haefeker, U. (2011) Quantum-mechanical calculations of the Raman spectra of Mg- and Fe-cordierite. American Mineralogist, 96(10), 1568-1574.
Kissel, L., and Pratt, R.H. (1990) Corrections to tabulated anomalous-scattering factors. Acta Crystallographica Section A: Foundations of Crystallography, 46(3), 170-175.
Koepke, J., and Schulz, H. (1986) Single crystal structure investigations under high-pressure of the mineral cordierite with an improved high-pressure cell. Physics and Chemistry of Minerals, 13(3), 165-173.
Kolesov, B.A., and Geiger, C.A. (2000) Cordierite II: The role of CO_2 and H_2O. American Mineralogist, 85(9), 1265-1274.
Likhacheva, A.Y., Goryainov, S.V., and Bul'bak, T.A. (2013) An X-ray diffraction study of the pressure-induced hydration in cordierite at 4–5 GPa. American Mineralogist, 98(1), 181-186.
Likhacheva, A.Y., Goryainov, S.V., Krylov, A.S., Bul'bak, T.A., and Prasad, P.S.R. (2011) Raman spectroscopy of natural cordierite at high water pressure up to 5 GPa. Journal of Raman Spectroscopy, 43(4), 559-563.
Malcherek, T., Domeneghetti, M.C., Tazzoli, V., Ottolini, L., McCammon, C., and Carpenter, M.A. (2001) Structural properties of ferromagnesian cordierites. American Mineralogist, 86(1-2), 66-79.
Martignole, J., and Sisi, J.-C. (1981) Cordierite-garnet-H_2O equilibrium: A geological thermometer, barometer and water fugacity indicator. Contributions to Mineralogy and Petrology, 77(1), 38-46.
Meagher, E.P., and Gibbs, G.V. (1977) The polymorphism of cordierite: II. The crystal structure of indialite. The Canadian Mineralogist, 15(1), 43-49.
Miletich, R., Gatta, G.D., Willi, T., Mirwald, P.W., Lotti, P., Merlini, M., Rotiroti, N., and Loerting, T. (2014a) Cordierite under hydrostatic compression: Anomalous elastic behavior as a precursor for a pressure-induced phase transition. American Mineralogist, 99(2-3), 479-493.
Miletich, R., Scheidl, K.S., Schmitt, M., Moissl, A.P., Pippinger, T., Gatta, G.D., Schuster, B., and Trautmann, C. (2014b) Static elasticity of cordierite I: Effect of heavy ion irradiation on the compressibility of hydrous cordierite. Physics and Chemistry of Minerals, 41(8), 579-591.

Mirwald, P.W. (1982) High-pressure phase transitions in cordierite. Physics of the Earth and Planetary Interiors, 29(1), 1-5.
Mirwald, P.W., Malinowski, M., and Schulz, H. (1984) Isothermal compression of low-cordierite to 30 kbar (25° C). Physics and Chemistry of Minerals, 11(3), 140-148.
Plonka, A.M., Dera, P., Irmen, P., Rivers, M.L., Ehm, L., and Parise, J.B. (2012) β-diopside, a new ultrahigh-pressure polymorph of $CaMgSi_2O_6$ with six-coordinated silicon. Geophysical Research Letters, 39(24).
Prencipe, M., Scanavino, I., Nestola, F., Merlini, M., Civalleri, B., Bruno, M., and Dovesi, R. (2011) High-pressure thermo-elastic properties of beryl ($Al_4Be_6Si_{12}O_{36}$) from ab initio calculations, and observations about the source of thermal expansion. Physics and Chemistry of Minerals, 38(3), 223-239.
Putnis, A. (1980a) The distortion index in anhydrous Mg-Cordierite. Contributions to Mineralogy and Petrology, 74(2), 135-141.
-. (1980b) Order-modulated structures and the thermodynamics of cordierite reactions. Nature, 287(5778), 128-131.
Putz, H., Schön, J.C., and Jansen, M. (1999) Combined method for ab initio structure solution from powder diffraction data. Journal of Applied Crystallography, 32(5), 864-870.
Ralph, R.L., Finger, L.W., Hazen, R.M., and Ghose, S. (1984) Compressibility and crystal structure of andalusite at high pressure. American Mineralogist, 69(5-6), 513-519.
Richet, P., and Gillet, P. (1997) Pressure-induced amorphization of minerals: A review. European Journal of Mineralogy, 9(5), 907-933.
Rivers, M., Prakapenka, V.B., Kubo, A., Pullins, C., Holl, C.M., and Jacobsen, S.D. (2008) The COMPRES/GSECARS gas-loading system for diamond anvil cells at the Advanced Photon Source. High Pressure Research, 28(3), 273-292.
Roy, R., Agrawal, D.K., and McKinstry, H.A. (1989) Very low thermal expansion coefficient materials. Annual Review of Materials Science, 19(1), 59-81.
Scheidl, K.S., Gatta, G.D., Pippinger, T., Schuster, B., Trautmann, C., and Miletich, R. (2014) Static elasticity of cordierite II: Effect of molecular CO2 channel constituents on the compressibility. Physics and Chemistry of Minerals, 41(8), 617-631.
Schreyer, W., and Schairer, J.F. (1961) Compositions and structural states of anhydrous Mg-cordierites: A re-investigation of the central part of the system $MgO–Al_2O_3–SiO_2$. Journal of Petrology, 2(3), 324-406.
Sheldrick, G.M. (2008) A short history of SHELX. Acta Crystallographica Section A: Foundations of Crystallography, 64(1), 112-122.
Smyth, J.R., and McCormick, T.C. (1995) Crystallographic data for minerals. In T.J. Ahrens, Ed. Mineral Physics & Crystallography: A Handbook of Physical Constants, p. 1-17. American Geophysical Union.
Stephenson, D.A., and Moore, P.B. (1968) The crystal structure of grandidierite, $(Mg,Fe)Al_3SiBO_9$. Acta Crystallographica Section B: Structural Crystallography and Crystal Chemistry, 24(11), 1518-1522.
Yu, Y.G., Angel, R.J., Ross, N.L., and Gibbs, G.V. (2013) Pressure impact on the structure, elasticity, and electron density distribution of $CaSi_2O_5$. Physical Review B, 87(18).
Zhang, J.S., Reynard, B., Montagnac, G., Wang, R.C., and Bass, J.D. (2013) Pressure-induced Pbca-$P2_1/c$ phase transition of natural orthoenstatite: Compositional effect and its geophysical implications. American Mineralogist, 98(5-6), 986-992.

Tables

Table 1. Chemical composition of cordierite sample

Element	Weight %
Mg	7.88(8)
Fe	1.21(6)
Al	18.39(10)
Si	23.66(15)
Na	0.100(9)
O	49.3(3)
Total	100.52

Table 2. Unit cell parameters and volumes of cordierite phases

Run #	Structure	Au *a* (Å)	P (GPa)	*a* (Å)	*b* (Å)	*c* (Å)	*α*°	*β*°	*γ*°	V (Å^3)
1[a]	Cordierite	N/A	0	17.0508(6)	9.7129(3)	9.3357(3)	90	90	90	1546.11(9)
2	Cordierite	4.0678(6)	1.37(7)	17.055(5)	9.6916(5)	9.3100(5)	90	90	90	1538.8(5)
3[a]	Cordierite II	4.02450(13)	7.52(3)	15.567(3)	9.6235(4)	9.0658(6)	89.963(5)	86.252(10)	90.974(8)	1355.0(2)
2	Cordierite II	4.0195(6)	8.30(10)	15.504(2)	9.589(3)	9.0414(5)	89.92(2)	86.153(6)	90.97(2)	1340.9(3)
2[a]	Cordierite III (P1)	3.9797(8)	15.22(15)	8.5191(19)	8.2448(3)	9.1627(4)	85.672(4)	85.986(7)	70.839(10)	605.48(14)
2	Cordierite III (C1)	3.9797(8)	15.22(15)	13.6619(8)	9.718(2)	9.1627(4)	89.847(7)	84.883(5)	91.977(9)	1211.0(3)

[a]Crystal structure refined at this pressure step

Table 3. Atomic parameters of cordierite at room pressure and 300 K

Site	Previous (Cohen et al.)	Coord. #	Wyckoff Position	x/*a*	y/*b*	z/*c*	Occupancy	U11	U22	U33	U23	U13	U12	U_{eq}
Mg1/ Fe1	M	6	8h	0.16265(4)	0.5	0.75	0.959(4)/ 0.041(4)	0.0064(4)	0.0062(4)	0.0083(4)	0.0001(3)	0	0	0.0070(3)
Al1	$T_1$1	4	8k	0.25	0.75	0.75006(7)	1	0.0085(3)	0.0060(3)	0.0073(3)	0	0	-0.0013(3)	0.00730(12)
Al2	$T_2$6	4	8l	0.94921(3)	0.69214(6)	0	1	0.0062(3)	0.0065(3)	0.0068(3)	0	0	0.0005(3)	0.00648(13)
Si1	$T_1$6	4	4a	0	0.5	0.75	1	0.0065(4)	0.0070(4)	0.0064(4)	0	0	0	0.00665(15)
Si2	$T_2$1	4	8l	0.19254(3)	0.07796(6)	0	1	0.0066(3)	0.0049(3)	0.0063(3)	0	0	0.00033(18)	0.00591(11)
Si3	$T_2$3	4	8l	0.13518(3)	0.76271(6)	0	1	0.0064(3)	0.0058(3)	0.0067(3)	0	0	-0.00077(18)	0.00630(11)
Ch1[a]	O_w	N/A	4b	0	0	0.75	0.78(5)	0.88(9)	0.160(19)	0.058(9)	0	0	0	0.37(3)
O1	$O_1$6		16m	0.06237(6)	0.58396(12)	0.65092(12)	1	0.0082(5)	0.0100(5)	0.0092(5)	0.0027(4)	-0.0005(4)	-0.0007(4)	0.0091(2)
O2	$O_2$1		8l	0.12241(10)	0.18458(18)	0	1	0.0112(7)	0.0104(8)	0.0165(8)	0	0	0.0038(6)	0.0127(4)
O3	$O_1$3		16m	0.17330(7)	0.68964(12)	0.85830(12)	1	0.0099(5)	0.0092(5)	0.0088(5)	-0.0022(4)	0.0023(4)	-0.0015(4)	0.0093(2)
O4	$O_1$1		16m	0.24728(7)	0.10297(12)	0.14122(12)	1	0.0118(5)	0.0076(5)	0.0086(5)	-0.0004(4)	-0.0024(4)	0.0009(4)	0.0093(2)
O5	$O_2$3		8l	0.16459(10)	0.92041(17)	0	1	0.0137(8)	0.0064(7)	0.0171(8)	0	0	-0.0027(6)	0.0124(3)
O6	$O_2$6		8l	0.04326(10)	0.75175(19)	0	1	0.0068(7)	0.0159(9)	0.0175(8)	0	0	-0.0018(6)	0.0134(4)

[a]Refined as oxygen.

Table 4. Atomic parameters of cordierite II at 7.52(3) GPa

Site	Coord. #	x/*a*	y/*b*	z/*c*	Occupancy	U_{iso}
Mg1A/ Fe1A	6	0.7102(16)	0.1491(14)	0.815(3)	0.959/ 0.041	0.0081(6)
Mg1B/ Fe1B	6	0.8481(12)	0.6506(12)	0.8172(17)	0.959/ 0.041	0.0081(6)
Mg1C/ Fe1C	6	0.8555(17)	0.5431(16)	0.319(3)	0.959/ 0.041	0.0081(6)
Mg1D/ Fe1D	6	0.6862(15)	0.0348(15)	0.338(3)	0.959/ 0.041	0.0081(6)
Mg1E/ Fe1E	6	0.1850(16)	0.5277(16)	0.855(3)	0.959/ 0.041	0.0081(6)
Mg1F/ Fe1F	6	0.3675(15)	0.0403(16)	0.818(3)	0.959/ 0.041	0.0081(6)
Mg1G/ Fe1G	6	0.3309(16)	0.9345(13)	0.368(3)	0.959/ 0.041	0.0081(6)
Mg1H/ Fe1H	6	0.2149(12)	0.4316(12)	0.3193(17)	0.959/ 0.041	0.0081(6)
Al1A	4	0.790(15)	0.8273(15)	0.844(3)	1	0.0055(6)
Al1B	5	0.8504(14)	0.3196(11)	0.806(3)	1	0.0055(6)
Al1C	4	0.7776(12)	0.2792(11)	0.3365(18)	1	0.0055(6)
Al1D	4	0.7629(15)	0.7862(14)	0.333(3)	1	0.0055(6)
Al1E	4	0.2752(14)	0.2908(14)	0.845(3)	1	0.0055(6)
Al1F	4	0.2707(12)	0.7842(11)	0.8460(19)	1	0.0055(6)
Al1G	5	0.1920(14)	0.7426(11)	0.364(3)	1	0.0055(6)
Al1H	4	0.3318(15)	0.2476(15)	0.336(3)	1	0.0055(6)
Al2A	4	0.5029(14)	0.2187(13)	0.015(3)	1	0.0016(5)
Al2B	4	0.5462(14)	0.8602(13)	0.157(3)	1	0.0016(5)
Al2C	4	0.5918(14)	0.2267(14)	0.621(3)	1	0.0016(5)
Al2D	4	0.4517(14)	0.8516(14)	0.556(3)	1	0.0016(5)
Al2E	4	0.9475(12)	0.7212(13)	0.0447(19)	1	0.0016(5)
Al2F	4	0.0862(12)	0.3566(13)	0.1432(19)	1	0.0016(5)
Al2G	4	0.0550(15)	0.7023(14)	0.649(3)	1	0.0016(5)
Al2H	4	0.9882(15)	0.3702(14)	0.521(3)	1	0.0016(5)
Si1A	5	0.5417(16)	0.9637(15)	0.821(3)	1	0.0114(8)
Si1B	5	0.0394(14)	0.6154(14)	0.318(3)	1	0.0114(8)
Si1C	5	0.0098(14)	0.4544(14)	0.856(3)	1	0.0114(8)
Si1D	5	0.5069(16)	0.1128(15)	0.345(3)	1	0.0114(8)
Si2A	4	0.3801(12)	0.4533(12)	0.0616(18)	1	0.0093(6)
Si2B	4	0.6755(12)	0.6263(12)	0.1169(18)	1	0.0093(6)
Si2C	4	0.7308(16)	0.4575(15)	0.608(3)	1	0.0093(6)
Si2D	4	0.3185(16)	0.6196(15)	0.554(3)	1	0.0093(6)
Si2E	4	0.8293(11)	0.9672(11)	0.0394(18)	1	0.0093(6)
Si2F	4	0.2344(11)	0.1161(11)	0.1068(18)	1	0.0093(6)
Si2G	4	0.1804(15)	0.9504(14)	0.629(3)	1	0.0093(6)

Si2H	4	0.8672(15)	0.1294(14)	0.538(3)	1	0.0093(6)
Si3A	4	0.3594(16)	0.7758(14)	0.114(3)	1	0.0103(6)
Si3B	4	0.6804(15)	0.2994(14)	0.070(3)	1	0.0103(6)
Si3C	4	0.6308(16)	0.7460(14)	0.571(3)	1	0.0103(6)
Si3D	4	0.4194(16)	0.3358(14)	0.590(3)	1	0.0103(6)
Si3E	4	0.9143(15)	0.2611(14)	0.104(3)	1	0.0103(6)
Si3F	4	0.1289(15)	0.8211(14)	0.069(3)	1	0.0103(6)
Si3G	4	0.1738(15)	0.2618(13)	0.580(3)	1	0.0103(6)
Si3H	4	0.8797(14)	0.8206(13)	0.578(3)	1	0.0103(6)
Ch1A[a]	N/A	0.524(9)	0.594(9)	0.757(14)	0.78	0.156(16)
Ch1B[a]	N/A	0.454(9)	0.518(9)	0.264(13)	0.78	0.156(16)
Ch1C[a]	N/A	0.980(9)	0.031(9)	0.773(14)	0.78	0.156(16)
Ch1D[a]	N/A	0.011(9)	0.965(9)	0.227(14)	0.78	0.156(16)
O1A		0.599(3)	0.083(3)	0.723(5)	1	0.0065(10)
O1B		0.932(3)	0.586(3)	0.946(4)	1	0.0065(10)
O1C		0.950(3)	0.384(3)	0.696(5)	1	0.0065(10)
O1D		0.561(3)	0.890(3)	0.988(5)	1	0.0065(10)
O1E		0.578(3)	0.981(3)	0.270(5)	1	0.0065(10)
O1F		0.471(3)	0.180(3)	0.179(5)	1	0.0065(10)
O1G		0.962(3)	0.501(3)	0.435(4)	1	0.0065(10)
O1H		0.078(3)	0.689(3)	0.477(5)	1	0.0065(10)
O1I		0.079(3)	0.568(3)	0.755(4)	1	0.0065(10)
O1J		0.471(3)	0.097(3)	0.914(5)	1	0.0065(10)
O1K		0.450(3)	0.898(3)	0.716(5)	1	0.0065(10)
O1L		0.087(3)	0.414(3)	0.966(5)	1	0.0065(10)
O1M		0.100(3)	0.486(3)	0.254(4)	1	0.0065(10)
O1N		0.948(3)	0.652(3)	0.198(5)	1	0.0065(10)
O1O		0.428(3)	0.981(3)	0.466(5)	1	0.0065(10)
O1P		0.589(3)	0.166(3)	0.448(5)	1	0.0065(10)
O2A		0.675(4)	0.308(3)	0.666(5)	1	0.0086(13)
O2B		0.452(3)	0.359(3)	0.983(5)	1	0.0086(13)
O2C		0.573(3)	0.711(3)	0.201(5)	1	0.0086(13)
O2D		0.927(3)	0.239(3)	0.471(5)	1	0.0086(13)
O2E		0.103(3)	0.836(3)	0.705(5)	1	0.0086(13)
O2F		0.880(3)	0.815(3)	0.984(4)	1	0.0086(13)
O2G		0.180(3)	0.267(3)	0.156(4)	1	0.0086(13)
O2H		0.360(4)	0.763(4)	0.518(5)	1	0.0086(13)
O3A		0.933(3)	0.316(3)	0.932(4)	1	0.0074(10)
O3B		0.622(3)	0.829(3)	0.739(5)	1	0.0074(10)
O3C		0.790(4)	0.802(3)	0.711(5)	1	0.0074(10)
O3D		0.768(3)	0.278(3)	0.926(4)	1	0.0074(10)
O3E		0.859(3)	0.353(3)	0.207(5)	1	0.0074(10)
O3F		0.120(3)	0.742(3)	0.217(4)	1	0.0074(10)
O3G		0.697(3)	0.836(3)	0.440(5)	1	0.0074(10)
O3H		0.413(3)	0.235(3)	0.426(5)	1	0.0074(10)
O3I		0.338(3)	0.874(3)	0.959(4)	1	0.0074(10)

O3J	0.194(3)	0.329(3)	0.749(5)	1	0.0074(10)
O3K	0.358(3)	0.230(3)	0.713(5)	1	0.0074(10)
O3L	0.196(3)	0.713(3)	0.963(5)	1	0.0074(10)
O3M	0.288(3)	0.782(3)	0.210(4)	1	0.0074(10)
O3N	0.697(3)	0.226(2)	0.214(4)	1	0.0074(10)
O3O	0.254(4)	0.280(4)	0.447(5)	1	0.0074(10)
O3P	0.844(3)	0.728(3)	0.417(5)	1	0.0074(10)
O4A	0.737(3)	0.978(3)	0.919(5)	1	0.0074(10)
O4B	0.714(3)	0.702(3)	0.948(4)	1	0.0074(10)
O4C	0.801(4)	0.473(4)	0.734(6)	1	0.0074(10)
O4D	0.833(4)	0.179(3)	0.694(5)	1	0.0074(10)
O4E	0.745(3)	0.642(3)	0.252(4)	1	0.0074(10)
O4F	0.325(3)	0.391(3)	0.232(4)	1	0.0074(10)
O4G	0.766(3)	0.426(3)	0.446(5)	1	0.0074(10)
O4H	0.785(3)	0.126(3)	0.435(5)	1	0.0074(10)
O4I	0.284(3)	0.428(3)	0.947(4)	1	0.0074(10)
O4J	0.271(3)	0.154(3)	0.966(4)	1	0.0074(10)
O4K	0.261(3)	0.929(3)	0.733(5)	1	0.0074(10)
O4L	0.264(3)	0.644(3)	0.724(5)	1	0.0074(10)
O4M	0.301(3)	0.108(3)	0.255(5)	1	0.0074(10)
O4N	0.768(3)	0.917(3)	0.243(4)	1	0.0074(10)
O4O	0.214(4)	0.905(3)	0.460(5)	1	0.0074(10)
O4P	0.244(4)	0.597(4)	0.439(6)	1	0.0074(10)
O5A	0.654(3)	0.457(3)	0.086(4)	1	0.0082(16)
O5B	0.384(3)	0.630(3)	0.049(4)	1	0.0082(16)
O5C	0.661(3)	0.577(3)	0.596(4)	1	0.0082(16)
O5D	0.374(3)	0.489(3)	0.552(4)	1	0.0082(16)
O5E	0.163(3)	0.971(3)	0.068(4)	1	0.0082(16)
O5F	0.877(3)	0.103(3)	0.079(4)	1	0.0082(16)
O5G	0.132(3)	0.089(3)	0.613(4)	1	0.0082(16)
O5H	0.903(3)	0.975(3)	0.532(4)	1	0.0082(16)
O6A	0.953(3)	0.716(3)	0.656(4)	1	0.0069(14)
O6B	0.604(3)	0.215(3)	0.996(4)	1	0.0069(14)
O6C	0.436(3)	0.851(3)	0.201(4)	1	0.0069(14)
O6D	0.090(3)	0.345(3)	0.494(4)	1	0.0069(14)
O6E	0.507(3)	0.319(3)	0.664(5)	1	0.0069(14)
O6F	0.041(3)	0.801(3)	0.986(4)	1	0.0069(14)
O6G	0.011(3)	0.250(3)	0.162(4)	1	0.0069(14)
AO6H	0.521(3)	0.742(3)	0.518(5)	1	0.0069(14)

All atoms are in Wyckoff position 1a.
[a]Refined as oxygen.

Table 5. Atomic parameters of cordierite III at 15.22(15) GPa

Site	Corresponding Sites in Cord. II	Coord. #	x/*a*	y/*b*	z/*c*	Occupancy	U_{iso}
Mg1A/ Fe1A	Mg1A, Mg1E/ Fe1A, Fe1E	5	0.610(4)	0.736(3)	0.7700(13)	0.959/ 0.041	0.0103(5)
Mg1B/ Fe1B	Mg1B, Mg1F/ Fe1B, Fe1F	6	0.228(4)	0.387(2)	0.7359(12)	0.959/ 0.041	0.0103(5)
Mg1C/ Fe1C	Mg1C, Mg1G/ Fe1C, Fe1G	5	0.423(4)	0.200(3)	0.2260(13)	0.959/ 0.041	0.0103(5)
Mg1D/ Fe1D	Mg1D, Mg1H/ Fe1D, Fe1H	5	0.791(4)	0.552(2)	0.2637(13)	0.959/ 0.041	0.0103(5)
Al1A	Al1A, Al1E	5	0.897(4)	0.4410(18)	0.7896(11)	1	0.0053(4)
Al1B	Al1B, Al1F	5	0.520(3)	0.0914(14)	0.7051(9)	1	0.0053(4)
Al1C	Al1D, Al1G	5	0.472(3)	0.8680(14)	0.2937(9)	1	0.0053(4)
Al1D	Al1D, Al1H	5	0.119(4)	0.5007(18)	0.2107(11)	1	0.0053(4)
Al2A	Al2A, Al2E	4	0.325(3)	0.5725(14)	0.9274(9)	1	0.0034(4)
Al2B	Al2B, Al2F	4	0.713(3)	0.3507(13)	0.0725(9)	1	0.0034(4)
Al2C	Al2C, Al2G	4	0.393(4)	0.6644(18)	0.5720(10)	1	0.0034(4)
Al2D	Al2D, Al2H	4	0.626(4)	0.2754(17)	0.4309(11)	1	0.0034(4)
Si1A	Si1A, Si1C	6	0.625(4)	0.3538(17)	0.7536(11)	1	0.0111(6)
Si1B	Si1B, Si1D	6	0.401(4)	0.5812(18)	0.2514(11)	1	0.0111(6)
Si2A	Si2A, Si2E	4	0.940(2)	0.7359(11)	0.9390(7)	1	0.0104(5)
Si2B	Si2B, Si2F	4	0.0850(19)	0.2292(11)	0.0478(7)	1	0.0104(5)
Si2C	Si2C, Si2G	4	0.265(4)	0.0490(18)	0.5453(12)	1	0.0104(5)
Si2D	Si2D, Si2H	4	0.756(4)	0.8894(18)	0.4559(12)	1	0.0104(5)
Si3A	Si3A, Si3E	5	0.642(4)	0.0447(19)	0.9915(11)	1	0.0116(5)
Si3B	Si3B, Si3F	5	0.383(4)	0.8976(18)	0.0136(10)	1	0.0116(5)
Si3C	Si3C, Si3G	5	0.934(4)	0.3394(17)	0.5116(10)	1	0.0116(5)
Si3D	Si3D, Si3H	5	0.074(4)	0.6110(17)	0.4898(10)	1	0.0116(5)
Ch1A[a]	Ch1A, Ch1C	N/A	0.99(3)	0.898(14)	0.759(9)	0.78	0.16(3)
Ch1B[a]	Ch1B, Ch1D	N/A	0.12(3)	0.940(15)	0.219(9)	0.78	0.16(3)
O1A	O1A, O1I		0.564(8)	0.570(5)	0.659(3)	1	0.0078(7)
O1B	O1B, O1J		0.427(7)	0.402(4)	0.839(3)	1	0.0078(7)

O1C	O1C, O1K	0.555(8)	0.271(4)	0.598(3)	1	0.0078(7)
O1D	O1D, O1L	0.722(8)	0.416(4)	0.905(3)	1	0.0078(7)
O1E	O1E, O1M	0.630(6)	0.520(4)	0.155(2)	1	0.0078(7)
O1F	O1F, O1N	0.307(7)	0.509(4)	0.100(3)	1	0.0078(7)
O1G	O1G, O1O	0.467(8)	0.363(5)	0.338(3)	1	0.0078(7)
O1H	O1H, O1P	0.445(8)	0.687(4)	0.403(3)	1	0.0078(7)
O2A	O2A, O2E	0.313(7)	0.851(4)	0.627(3)	1	0.0119(13)
O2B	O2B, O2F	0.141(5)	0.642(3)	0.8608(16)	1	0.0119(13)
O2C	O2C, O2G	0.892(5)	0.254(3)	0.1289(16)	1	0.0119(13)
O2D	O2D, O2H	0.706(8)	0.078(4)	0.381(3)	1	0.0119(13)
O3A	O3A, O3I	0.658(9)	0.140(5)	0.830(3)	1	0.0101(8)
O3B	O3B, O3J	0.824(8)	0.323(5)	0.687(3)	1	0.0101(8)
O3C	O3C, O3K	0.018(8)	0.462(5)	0.631(3)	1	0.0101(8)
O3D	O3D, O3L	0.516(7)	0.945(4)	0.883(3)	1	0.0101(8)
O3E	O3E, O3M	0.509(8)	0.980(4)	0.124(3)	1	0.0101(8)
O3F	O3F, O3N	0.357(9)	0.804(5)	0.173(3)	1	0.0101(8)
O3G	O3G, O3O	0.007(8)	0.467(4)	0.372(3)	1	0.0101(8)
O3H	O3H, O3P	0.174(8)	0.623(5)	0.315(3)	1	0.0101(8)
O4A	O4A, O4I	0.828(6)	0.644(4)	0.8314(17)	1	0.0089(8)
O4B	O4B, O4J	0.056(7)	0.337(4)	0.889(3)	1	0.0089(8)
O4C	O4C, O4K	0.305(7)	0.168(4)	0.6567(19)	1	0.0089(8)
O4D	O4D, O4L	0.627(8)	0.901(5)	0.605(3)	1	0.0089(8)
O4E	O4E, O4M	0.187(6)	0.289(4)	0.1855(18)	1	0.0089(8)
O4F	O4F, O4N	0.960(7)	0.588(4)	0.112(3)	1	0.0089(8)
O4G	O4G, O4O	0.380(8)	0.036(5)	0.396(3)	1	0.0089(8)
O4H	O4H, O4P	0.690(7)	0.792(4)	0.333(2)	1	0.0089(8)
O5A	O5A, O5E	0.214(7)	0.037(4)	0.981(3)	1	0.0167(14)
O5B	O5B, O5F	0.836(7)	0.916(4)	0.015(2)	1	0.0167(14)
O5C	O5C, O5G	0.096(9)	0.127(5)	0.500(3)	1	0.0167(14)
O5D	O5D, O5H	0.948(9)	0.809(5)	0.498(3)	1	0.0167(14)
O6A	O6A, O6E	0.252(7)	0.573(4)	0.587(3)	1	0.0094(11)
O6B	O6B, O6F	0.409(7)	0.717(4)	0.912(3)	1	0.0094(11)
O6C	O6C, O6G	0.598(7)	0.222(4)	0.081(3)	1	0.0094(11)

O6D	O6D, O6H	0.736(7)	0.391(4)	0.415(3)	1	0.0094(11)

All atoms are in Wyckoff position 1a.
[a]Refined as oxygen.

Table 6. Details of crystal structure refinements

a) Cordierite

Facility	IMSERC, Northwestern
Wavelength, Å	0.71073
Pressure, GPa	10^{-4}
Temperature, K	298
Symmetry	Orthorhombic, *Cccm*
Lattice Parameters *a*, *b*, *c*, Å	17.0508(6), 9.7129(3), 9.3357(3)
Volume, $Å^3$	1546.11(9)
Z	4
Reflection Range	$-28 \leq h \leq 28$, $-16 \leq k \leq 14$, $-15 \leq l \leq 15$
Maximum θ, °	72.70
Number Independent Reflections	1981
Number Refined Parameters	82
Refinement	F^2
R1	0.0330
wR_2	0.0808
GooF	1.088

b) Cordierite II

HPCAT	16 ID-B, HPCAT, APS, ANL
Wavelength, Å	0.35145
Pressure, GPa	7.52(3)
Temperature, K	298
Symmetry	Triclinic, *P*1
Lattice Parameters *a*, *b*, *c* (Å)	15.567(3), 9.6235(4), 9.0659(6)
Lattice Parameters α, β, γ (°)	89.963(5), 86.252(10), 90.974(9)
Volume, $Å^3$	1355.0(2)
Z	4
Reflection Range	$-20 \leq h \leq 19$, $-14 \leq k \leq 14$, $-13 \leq l \leq 12$
Maximum θ, °	31.78
Number Independent Reflections	3350
Number Refined Parameters	374
Refinement	F^2
R1	0.0722
wR_2	0.1780
GooF	1.057

c) Cordierite III

Facility	16 ID-B, HPCAT, APS, ANL
Wavelength, Å	0.30622
Pressure, GPa	15.22(15)
Temperature, K	298
Symmetry	Triclinic, *P*1
Lattice Parameters *a*, *b*, *c*, Å	8.5191(19), 8.2448(3), 9.1627(4)
Lattice Parameters *α, β, γ* (°)	85.672(4), 85.986(8), 70.839(11)
Volume, $Å^3$	605.5(2)
Z	2
Reflection Range	$-11 \leq h \leq 10$, $-13 \leq k \leq 13$, $-16 \leq l \leq 16$
Maximum θ, °	33.99
Number Independent Reflections	1844
Number Refined Parameters	194
Refinement	F^2
R1	0.0644
wR_2	0.1633
GooF	1.075

Table 7. Geometry of selected coordination polyhedra in cordierite and its high-pressure polymorphs

a) M1 layer

Site	Phase	Coordination Geometry	Angle Name	Angle (°)	Axial/ Radial	Bond	Bond Length (Å)	Axial/Radial/Broken
Mg1	Cordierite	Octahedron	O4-Mg1-O1	172.65(5)	N/A	Mg1-O4	2.0952(12)	N/A
			O3-Mg1-O3	170.13(7)	N/A	Mg1-O1	2.1081(12)	N/A
						Mg1-O3	2.1090(11)	N/A
Mg1A	Cordierite II	Octahedron	O4A-Mg1A-O2A	168.2(1.4)	N/A	Mg1A-O4A	1.96(3)	N/A
			O4D-Mg1A-O6B	152.0(1.3)	N/A	Mg1A-O2A	2.14(4)	N/A
			O3D-Mg1A-O1A	149.8(1.8)	N/A	Mg1A-O4D	2.16(6)	N/A
						Mg1A-O6B	2.31(5)	N/A
						Mg1A-O3D	1.85(3)	N/A
						Mg1A-O1A	2.06(4)	N/A
						Mg1A-O1D	3.66[a]	B
						Mg1A-O3B	3.44[a]	B
Mg1E	Cordierite II	Octahedron	O4I-Mg1E-O1I	163.3(1.4)	N/A	Mg1E-O4I	2.05(4)	N/A
			O4L-Mg1E-O1L	170.1(1.2)	N/A	Mg1E-O1I	1.98(4)	N/A
			O3L-Mg1E-O3J	171.0(1.8)	N/A	Mg1E-O4L	1.98(6)	N/A
						Mg1E-O1L	2.07(6)	N/A
						Mg1E-O3L	2.04(4)	N/A
						Mg1E-O3J	2.14(4)	N/A
Mg1B	Cordierite II	Octahedron	O4C-Mg1B-O2F	160(3)	N/A	Mg1B-O4C	2.01(4)	N/A
			O4B-Mg1B-O6A	148.6(1.1)	N/A	Mg1B-O2F	2.26(3)	N/A
			O3C-Mg1B-O1B	152.0(1.5)	N/A	Mg1B-O4B	2.39(6)	N/A
						Mg1B-O6A	2.21(6)	N/A
						Mg1B-O3C	2.00(3)	N/A
						Mg1B-O1B	1.92(3)	N/A
						Mg1B-O1C	3.20[a]	B
						Mg1B-O3A	3.68[a]	B
Mg1F	Cordierite II	Octahedron	O4K-Mg1F-O1J	166.0(1.3)	N/A	Mg1F-O4K	2.15(4)	N/A
			O4J-Mg1F-O1K	166.6(1.7)	N/A	Mg1F-O1J	1.95(4)	N/A
			O3K-Mg1F-O3I	160(3)	N/A	Mg1F-O4J	2.24(5)	N/A
						Mg1F-O1K	2.07(5)	N/A
						Mg1F-O3K	2.07(4)	N/A
						Mg1F-O3I	2.08(4)	N/A
Mg1A	Cordierite III	Square Pyramid	O4A-Mg1A-O1A	109(3)	A	Mg1A-O4A	1.86(6)	A
			O4A-Mg1A-O6B	119.7(1.5)	A	Mg1A-O1A	1.92(3)	R

			O4A-Mg1A-O3D	103.2(1.8)	A	Mg1A-O6B	2.12(5)	R
			O4A-Mg1A-O4D	104(3)	A	Mg1A-O3D	1.98(4)	R
			O3D-Mg1A-O1A	146(3)	R	Mg1A-O4D	1.99(3)	R
			O4D-Mg1A-O6B	133(3)	R	Mg1A-O2A	2.78 [a]	B
Mg1B	Cordierite III	Octahedron	O4C-Mg1B-O2B	173.3(1.1)	N/A	Mg1B-O4C	1.89(4)	N/A
			O4B-Mg1B-O6A	140(3)	N/A	Mg1B-O2B	2.34(3)	N/A
			O3C-Mg1B-O1B	159.6(1.3)	N/A	Mg1B-O4B	2.07(4)	N/A
						Mg1B-O6A	2.03(3)	N/A
						Mg1B-O3C	1.98(7)	N/A
						Mg1B-O1B	2.05(5)	N/A
Si1	Cordierite	Rhombic Disphenoid	O1-Si1-O1	119.89(8)	N/A	Si1-O1	1.6284(11)	N/A
			O1-Si1-O1	110.77(8)				
			O1-Si1-O1	98.45(8)				
Si1A	Cordierite II	Trigonal Bipyramid	O3B-Si1A-O1J	174.8(1.3)	A	Si1A-O3B	1.93(5)	A
			O1D-Si1A-O1A	129.4(1.8)	R	Si1A-O1J	1.88(5)	A
			O1D-Si1A-O1K	120(2)	R	Si1A-O1D	1.72(4)	R
			O1A-Si1A-O1K	110.6(1.8)	R	Si1A-O1A	1.67(5)	R
						Si1A-O1K	1.88(4)	R
Si1C	Cordierite II	Trigonal Bipyramid	O3A-Si1C-O1I	170.0(1.8)	A	Si1C-O3A	1.87(5)	A
			O1B-Si1C-O1C	103.7(1.5)	R	Si1C-O1I	1.73(5)	A
			O1B-Si1C-O1L	111.6(1.8)	R	Si1C-O1B	1.91(5)	R
			O1C-Si1C-O1L	141.7(1.6)	R	Si1C-O1C	1.89(3)	R
						Si1C-O1L	1.67(3)	R
Si1A	Cordierite III	Octahedron	O3A-Si1A-O1A	171(3)	N/A	Si1A-O3A	1.79(3)	N/A
			O3B-Si1A-O1B	172.2(1.2)	N/A	Si1A-O1A	1.85(4)	N/A
			O1C-Si1A-O1D	173(3)	N/A	Si1A-O3B	1.71(7)	N/A
						Si1A-O1B	1.74(5)	N/A
						Si1A-O1C	1.84(3)	N/A
						Si1A-O1D	1.84(4)	N/A
Al1	Cordierite	Rhombic disphenoid	O4-Al1-O4	109.16(9)	N/A	Al1-O4	1.7533(12)	N/A
			O4-Al1-O3	125.91(5)	N/A	Al1-O3	1.7536(12)	N/A
			O4-Al1-O3	94.66(5)	N/A			
			O3-Al1-O3	109.64(9)	N/A			
Al1A	Cordierite II	Tetrahedron	O4B-Al1A-O4A	113.8(1.7)	N/A	Al1A-O4B	1.54(4)	N/A
			O4B-Al1A-O3C	104(3)	N/A	Al1A-O4A	1.66(3)	N/A
			O4B-Al1A-O3B	116(3)	N/A	Al1A-O3C	1.71(7)	N/A
			O3C-Al1A-O4A	103(3)	N/A	Al1A-O3B	1.71(4)	N/A
			O3C-Al1A-O3B	101(3)	N/A			
			O4A-Al1A-O3B	116.7(1.6)	N/A			
Al1E	Cordierite II	Rhombic disphenoid	O4J-Al1E-O4I	105.0(1.8)	N/A	Al1E-O4J	1.71(4)	N/A

			O4J-Al1E-O3K	99.3(1.9)	N/A	Al1E-O4I	1.62(3)	N/A
			O4J-Al1E-O3J	122(3)	N/A	Al1E-O3K	1.81(6)	N/A
			O3K-Al1E-O4I	124(3)	N/A	Al1E-O3J	1.63(4)	N/A
			O3K-Al1E-O3J	106(3)	N/A			
			O4I-Al2A-O3J	102.0(1.6)	N/A			
Al1B	Cordierite II	Trigonal Bipyramid	O3D-Al1B-O1C	170.7(1.5)	A	Al1B-O3D	1.67(5)	A
			O3A-Al1B-O4C	126.7(1.4)	R	Al1B-O1C	1.89(6)	A
			O3A-Al1B-O4D	120.0(1.5)	R	Al1B-O3A	1.78(3)	R
			O4C-Al1B-O4D	110.4(1.5)	R	Al1B-O4C	1.82(4)	R
						Al1B-O4D	1.72(4)	R
Al1F	Cordierite II	Rhombic disphenoid	O4L-Al1F-O4K	103.5(1.6)	N/A	Al1F-O4L	1.76(4)	N/A
			O4L-Al1F-O3L	91(2)	N/A	Al1F-O4K	1.74(3)	N/A
			O4L-Al1F-O3I	144(1.8)	N/A	Al1F-O3L	1.66(6)	N/A
			O3L-Al1F-O4K	128(2)	N/A	Al1F-O3I	1.73(3)	N/A
			O3L-Al1F-O3I	103.9(1.9)	N/A			
			O4K-Al1F-O3I	92.2(1.3)	N/A			
Al1A	Cordierite III	Square Pyramid	O3B-Al1A-O4B	117(2)	A	Al1A-O4B	1.64(5)	A
			O4A-Al1A-O4B	109.2(1.6)	A	Al1A-O3B	1.68(3)	R
			O3C-Al1A-O4B	95(3)	A	Al1A-O4A	1.65(3)	R
			O1D-Al1A-O4B	102.2(1.8)	A	Al1A-O3C	1.75(5)	R
			O3C-Al1A-O1D	159(3)	R	Al1A-O1D	1.83(5)	R
			O3B-Al1A-O4A	133(3)	R			
Al1B	Cordierite III	Square Pyramid	O3A-Al1B-O4D	112(3)	A	Al1B-O4D	1.82(5)	A
			O4C-Al1B-O4D	108.1(1.9)	A	Al1B-O3A	1.86(5)	R
			O3D-Al1B-O4D	89.8(1.4)	A	Al1B-O4C	1.80(6)	R
			O1C-Al1B-O4D	106.4(1.6)	A	Al1B-O3D	1.95(3)	R
			O3D-Al1B-O1C	155.2(1.3)	R	Al1B-O1C	1.81(3)	R
			O3A-Al1B-O4C	140(3)	R			

[a]Uncertainty not calculated by SHELX

b) T1 layer

Site	Phase	Coordination Geometry	Angle Name	Angle (°)	Axial/ Radial	Bond	Bond Length (Å)	Axial/Radial/Broken
Si3	Cordierite	Tetrahedron	O5-Si3-O3	106.78(6)	N/A	Si3-O5	1.6117(18)	N/A
			O5-Si3-O6	112.02(10)	N/A	Si3-O3	1.6359(12)	N/A
			O3-Si3-O3	107.95(8)	N/A	Si3-O6	1.5709(17)	N/A
			O3-Si3-O6	111.51(5)	N/A			
Si3A	Cordierite II	Tetrahedron	O5B-Si3A-O3I	104.0(1.6)	N/A	Si3A-O5B	1.56(3)	N/A
			O5B-Si3A-O6C	113.4(1.9)	N/A	Si3A-O3I	1.75(3)	N/A
			O5B-Si3A-O3M	117(3)	N/A	Si3A-O6C	1.64(3)	N/A
			O3I-Si3A-O6C	110.1(1.7)	N/A	Si3A-O3M	1.36(5)	N/A
			O3I-Si3A-O3M	106.9(1.9)	N/A			
			O6C-Si3A-O3M	105(3)	N/A			
Si3E	Cordierite II	Tetrahedron	O5F-Si3E-O3A	101.8(1.8)	N/A	Si3E-O5F	1.64(4)	N/A
			O5F-Si3E-O6G	108.2(1.5)	N/A	Si3E-O3A	1.65(5)	N/A
			O5F-Si3E-O3E	116(3)	N/A	Si3E-O6G	1.63(4)	N/A
			O3A-Si3E-O6G	103(3)	N/A	Si3E-O3E	1.52(5)	N/A
			O3A-Si3E-O3E	116.9(1.8)	N/A			
			O6G-Si3E-O3E	110.3(1.8)	N/A			
Si3B	Cordierite II	Tetrahedron	O5A-Si3B-O3D	111(2)	N/A	Si3B-O5A	1.58(3)	N/A
			O5A-Si3B-O6B	108.8(1.7)	N/A	Si3B-O3D	1.84(5)	N/A
			O5A-Si3B-O3N	115.8(1.7)	N/A	Si3B-O6B	1.61(4)	N/A
			O3D-Si3B-O6B	100(3)	N/A	Si3B-O3N	1.52(4)	N/A
			O3D-Si3B-O3N	112.8(1.8)	N/A			
			O6B-Si3B-O3N	107.5(1.9)	N/A			
Si3F	Cordierite II	Tetrahedron	O5E-Si3F-O3L	112(3)	N/A	Si3F-O5E	1.53(4)	N/A
			O5E-Si3F-O6F	113.6(1.5)	N/A	Si3F-O3L	1.74(5)	N/A
			O5E-Si3F-O3F	118.7(1.8)	N/A	Si3F-O6F	1.61(3)	N/A
			O3L-Si3F-O6F	100.3(1.7)	N/A	Si3F-O3F	1.54(5)	N/A
			O3L-Si3F-O3F	101.3(1.8)	N/A			
			O6F-Si3F-O3F	109(3)	N/A			
Si3A	Cordierite III	Square Pyramid	O3D-Si3A-O5B	113.1(1.8)	A	Si3A-O5B	1.67(6)	A
			O3A-Si3A-O5B	102(3)	A	Si3A-O3D	1.91(4)	R
			O6C-Si3A-O5B	112(3)	A	Si3A-O3A	1.64(3)	R
			O3E-Si3A-O5B	108.4(1.9)	A	Si3A-O6C	1.65(3)	R
			O3D-Si3A-O6C	135(3)	R	Si3A-O3E	1.77(4)	R
			O3A-Si3A-O3E	147(4)	R			
Si3B	Cordierite III	Square Pyramid	O3E-Si3B-O5A	111.2(1.8)	A	Si3B-O5A	1.56(6)	A

O3D-Si3B-O5A	103.1(1.9)	A	Si3B-O3E	1.83(4)	R
O6B-Si3B-O5A	110(3)	A	Si3B-O3D	1.70(5)	R
O3F-Si3B-O5A	106(3)	A	Si3B-O6B	1.76(3)	R
O3E-Si3B-O6B	138(3)	R	Si3B-O3F	1.64(3)	R
O3D-Si3B-O3F	149(4)	R			

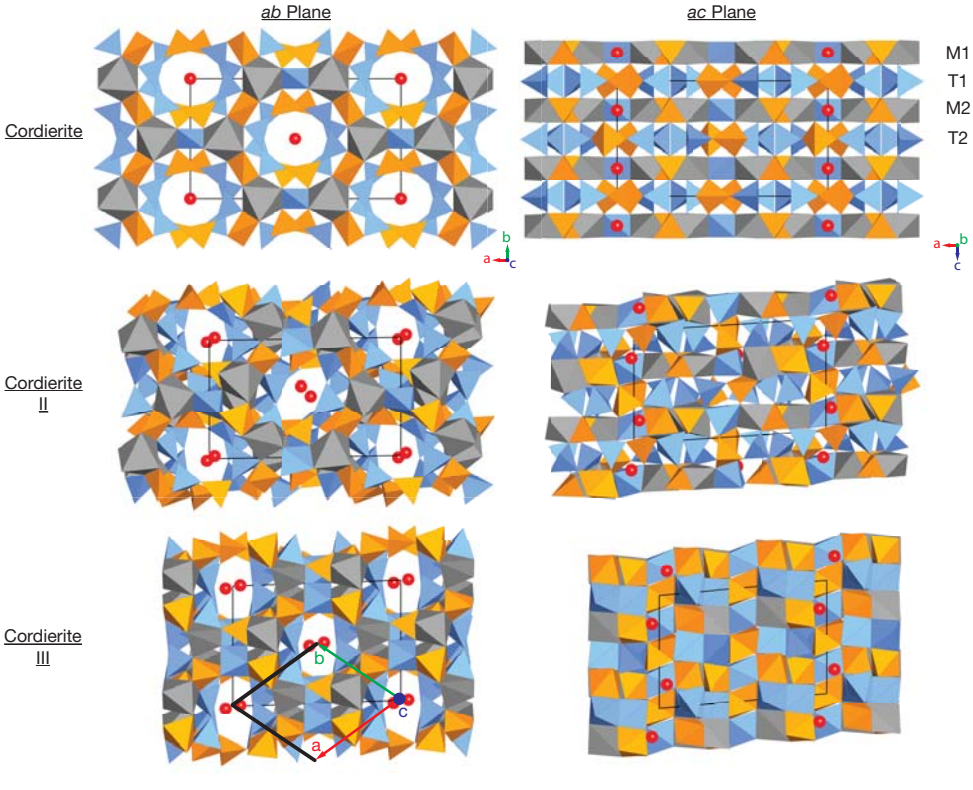
ab Plane
ac Plane
Cordierite
M1
T1
M2
T2
b
a
c
Cordierite
II
Cordierite
III
b
c
a

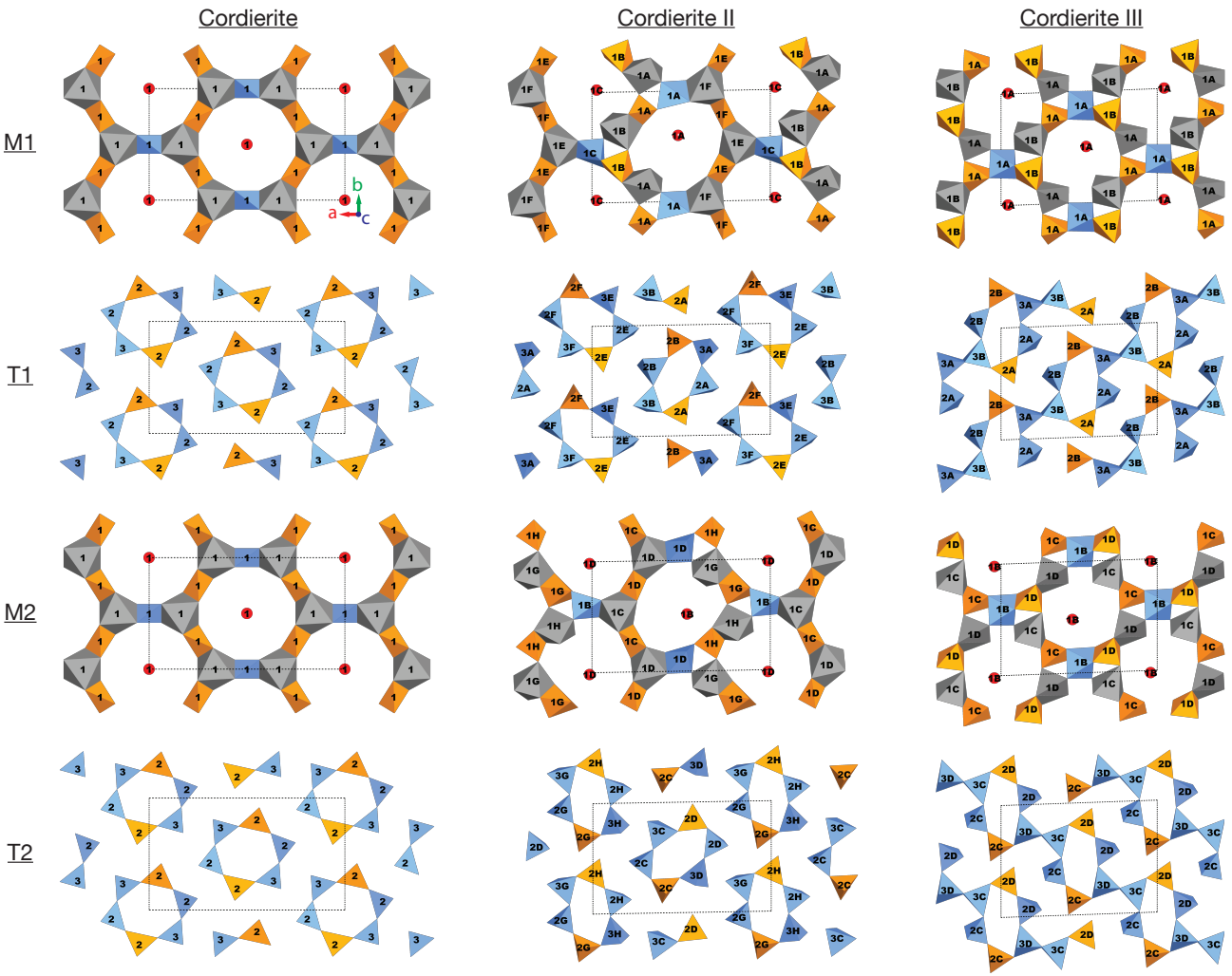
Cordierite
Cordierite II
Cordierite III
M1
T1
M2
T2
b
a
c

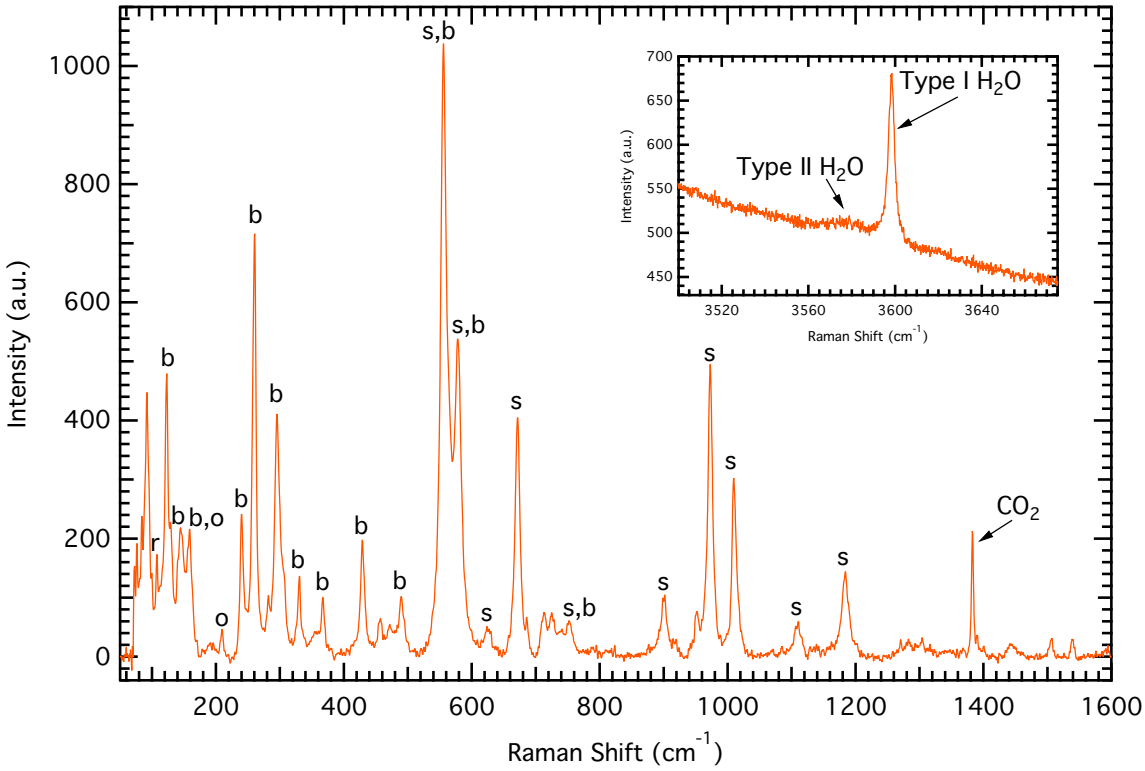
Intensity (a.u.)
Raman Shift (cm-1)
0
200
400
600
800
1000
200
400
600
800
1000
1200
1400
1600
r
b
b
b,o
o
b
b
b
b
b
b
s,b
s,b
s
s
s,b
s
s
s
s
s
CO2
Type I H2O
Type II H2O
Intensity (a.u.)
Raman Shift (cm-1)
450
500
550
600
650
700
3520
3560
3600
3640

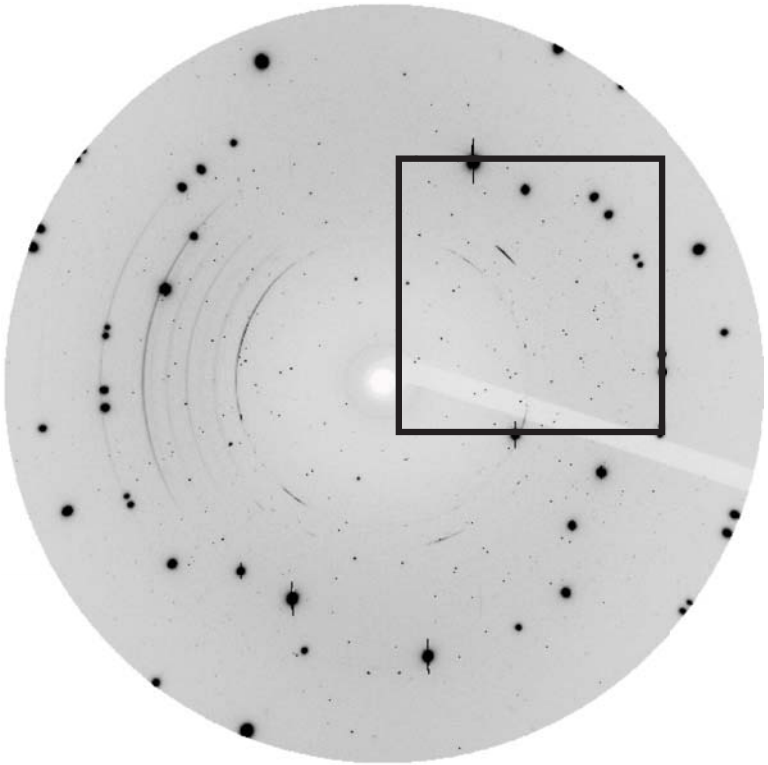

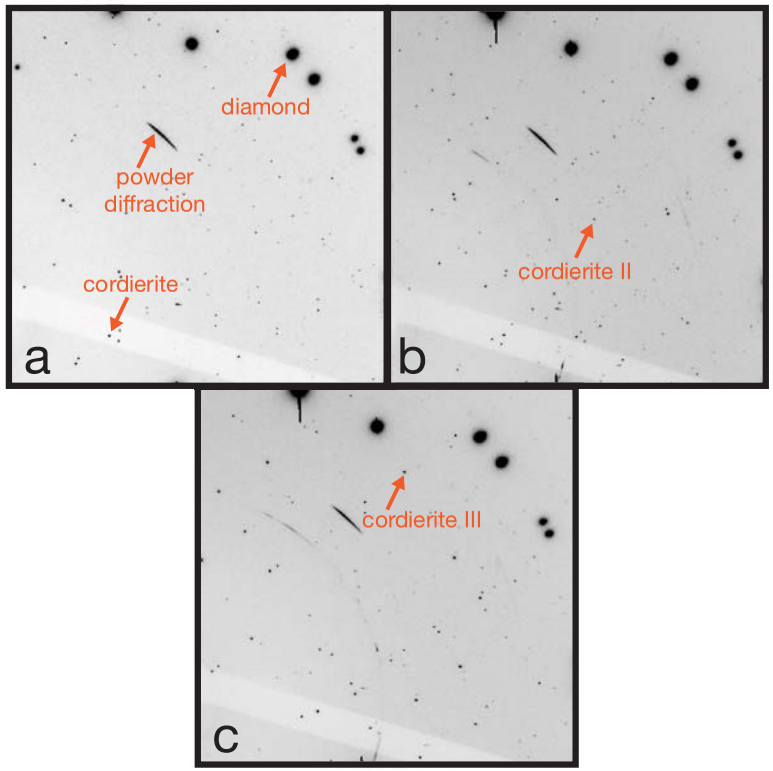
diamond
powder
diffraction
cordierite
a
cordierite II
b
cordierite III
c

a)

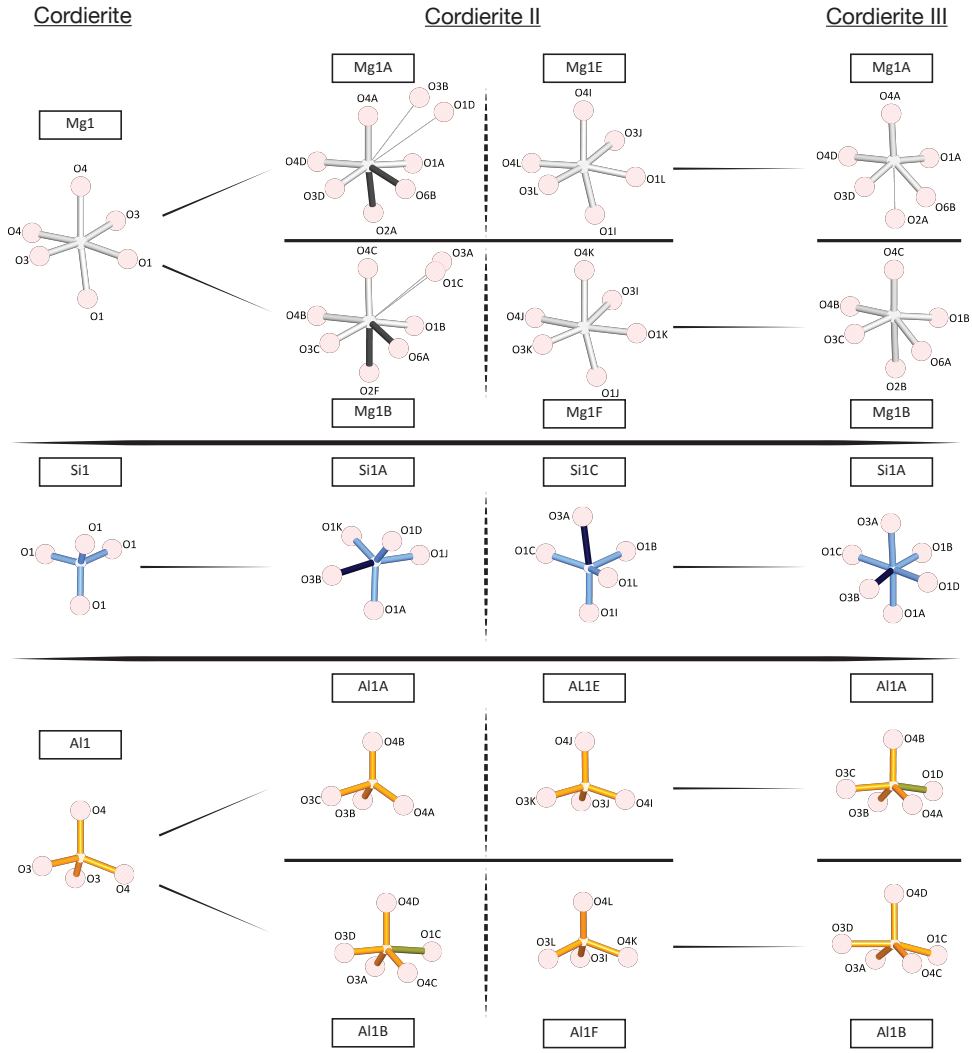
Cordierite
Cordierite II
Cordierite III
Mg1
Mg1A
Mg1E
Mg1A
Mg1B
Mg1F
Mg1B
Si1
Si1A
Si1C
Si1A
Al1
Al1A
AL1E
Al1A
Al1B
Al1F
Al1B

b)

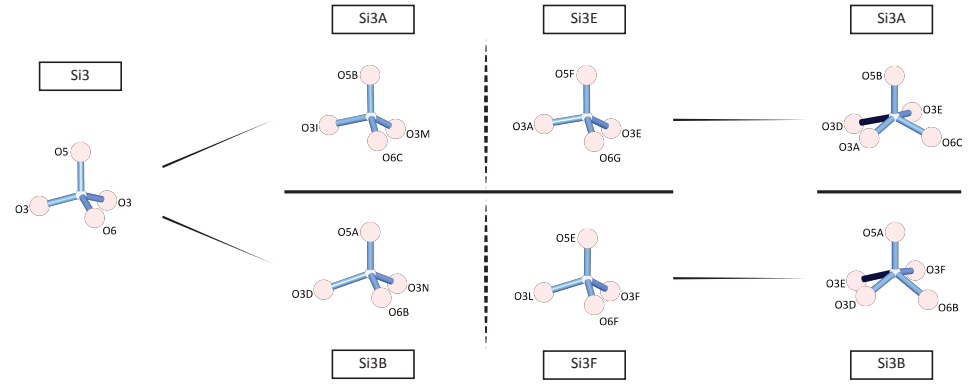
Si3
Si3A
Si3E
Si3A
Si3B
Si3F
Si3B

ab Plane

ac Plane

Cordierite

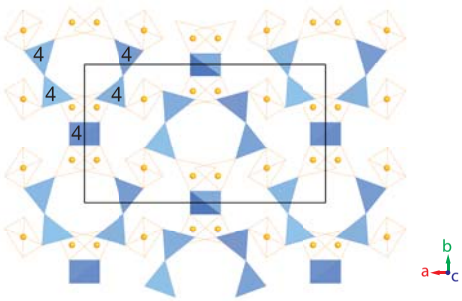

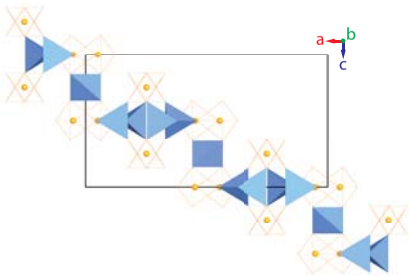

Cordierite
II

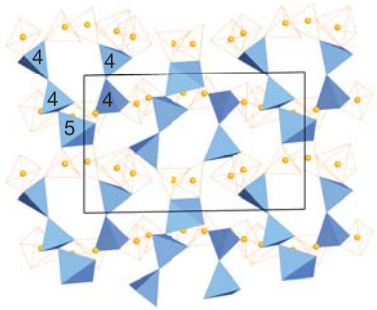

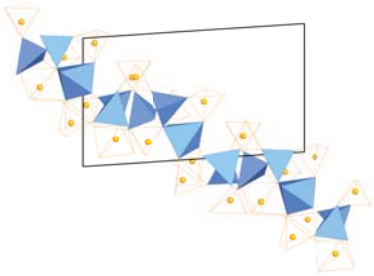

Cordierite
III